RESEARCH ARTICLE

WILEY

Estimating water balance components in irrigated agriculture using a combined approach of soil moisture and energy balance monitoring, and numerical modelling

Stephan Schulz[1] | Rike Becker[1,2] | Juan Carlos Richard-Cerda[1] | Muhammad Usman[3] | Tim aus der Beek[2] | Ralf Merz[4] | Christoph Schüth[1,2]

[1]Institute of Applied Geosciences, Technische Universität Darmstadt, Darmstadt, Germany

[2]Water Resources Management, IWW Institute for Water Research of Rhineland Westphalia, Mülheim an der Ruhr, Germany

[3]Department of Geoecology, Martin Luther University Halle-Wittenberg, Halle, Germany

[4]Department of Catchment Hydrology, Helmholtz-Centre for Environmental Research—UFZ, Halle, Germany

Correspondence
Stephan Schulz, Institute of Applied Geosciences, Technische Universität Darmstadt, Schnittspahnstr. 9, Darmstadt, Hessen 64287, Germany.
Email: schulz@geo.tu-darmstadt.de

Abstract

Information on water balance components such as evapotranspiration and groundwater recharge are crucial for water management. Due to differences in physical conditions, but also due to limited budgets, there is not one universal best practice, but a wide range of different methods with specific advantages and disadvantages. In this study, we propose an approach to quantify actual evapotranspiration, groundwater recharge and water inflow, i.e. precipitation and irrigation, that considers the specific conditions of irrigated agriculture in warm, arid environments. This approach does not require direct measurements of precipitation or irrigation quantities and is therefore suitable for sites with an uncertain data basis. For this purpose, we combine soil moisture and energy balance monitoring, remote sensing data analysis and numerical modelling using Hydrus. Energy balance data and routine weather data serve to estimate ET_0. Surface reflectance data from satellite images (Sentinel-2) are used to derive leaf area indices, which help to partition ET_0 into energy limited evaporation and transpiration. Subsequently, first approximations of water inflow are derived based on observed soil moisture changes. These inflow estimates are used in a series of forward simulations that produce initial estimates of drainage and ET_{act}, which in turn help improve the estimate of water inflow. Finally, the improved inflow estimates are incorporated into the model and then a parameter optimization is performed using the observed soil moisture as the reference figure. Forward simulations with calibrated soil parameters result in final estimates for ET_{act} and groundwater recharge. The presented method is applied to an agricultural test site with a crop rotation of cotton and wheat in Punjab, Pakistan. The final model results, with an RMSE of 2.2% in volumetric water content, suggest a cumulative ET_{act} and groundwater recharge of 769 and 297 mm over a period of 281 days, respectively. The total estimated water inflow accounts for 946 mm, of which 77% originates from irrigation.

KEYWORDS
actual evapotranspiration, ground heat flux, groundwater recharge, Hydrus, irrigation, net radiation, Sentinel-2, soil moisture

1 | INTRODUCTION

Information on water balance components is essential in hydrological sciences and related disciplines. It is needed to quantify the replenishment of natural resources and thus forms the basis for sustainable water resources management. For irrigated agricultural systems it helps in irrigation and drainage planning and in distinguishing between blue and green water footprints of crops.

Unfortunately, the possibilities for direct measurements of some balance components such as actual evapotranspiration (Allen et al., 2011; Wang & Dickinson, 2012) and groundwater recharge (Healy, 2010) are quite limited. Therefore, indirect approaches that require less own measurement effort are more frequently applied. Very common for the approximation of actual evapotranspiration (ET_{act}) is, for example, the Penman–Monteith equation, which uses routine weather data and information on plant physiology, usually extracted from readily accessible databases (Allen et al., 1998). Indirect methods for estimating groundwater recharge (GWR) include for instance hydrograph analysis, various tracer methods and modelling. Hydrological models are particularly interesting because they usually provide estimates of all water balance components. However, the reliability of their results depends strongly on the availability and quality of the input data, which therefore constitute the principal source for uncertainties, particularly in data scarce regions.

In addition to ET_{act} and GWR, natural water inflow, that is, precipitation, can also be subject to uncertainties, for instance if there are no precipitation measuring stations in the vicinity or if only spatially integrated data from satellite data (e.g., TRMM, CMORPH) or reanalysis (e.g., ERA5) are available. If imprecise precipitation estimates are then used in models, incorrect parameter estimates and model results may occur (Fraga et al., 2019; Peters-Lidard et al., 2008; Troutman, 1983). For irrigated agricultural systems, irrigation water is also an important but often insufficiently known inflow component (Brocca et al., 2018; Lankford, 2006; Wisser et al., 2008). The degree of uncertainty depends on the type of irrigation. In systems where the water is distributed by a piping system, equipped with flow meters, fairly accurate application rates are available. In many parts of the world, however, there are more rudimentary systems. For example, simple, hand-dug channels for water distribution are very common. Here, flow rates and transmission losses are often only roughly estimated, based on visual observations, irrigation schedules, and experience (Forkutsa et al., 2009). Irrigation rates become even more uncertain in case of excess irrigation. Here, in addition to inflow rates, drainage rates are required to calculate the net water input into the soil.

Motivated by the problem of inaccurate or unavailable precipitation measurements, Brocca et al. (2013) developed an approach to estimate precipitation amounts by analysing soil moisture changes. To do this, they inverted the soil water balance equation. Water balance components required in addition to soil moisture change were either neglected (evapotranspiration and surface runoff) or estimated using empirical methods (drainage). Soil moisture changes can be derived from in situ observations (Brocca et al., 2015) or from satellite-based radar data (Brocca et al., 2014). Later, this approach was also used to estimate irrigation volumes (Brocca et al., 2018; Dari et al., 2020; Filippucci et al., 2020).

The aim of the present study is to present a method that allows a reliable estimation of the water balance components ET_{act}, GWR, and water inflow (precipitation and irrigation) with moderate measurement efforts. This approach is particular suitable for irrigated areas, where irrigation water inflows are insufficiently known and difficult to measure. For this purpose, we apply a combined approach of soil moisture and radiation balance monitoring, remote sensing data analysis, and numerical modelling. Unknown irrigation amounts are estimated based on soil moisture data and an inversion of the soil water balance equation. This is accompanied by an iterative process in which other required water balance components are estimated stepwise by numerical modelling using Hydrus (Šimůnek et al., 2008).

2 | STUDY SITE

We apply this approach to an agricultural test field of the University of Agriculture Faisalabad in Punjab, Pakistan, which is part of the Lower Chenab Canal (LCC) system (Figure 1; Becker et al., 2019). The test field has a dimension of 110 m × 30 m and the crop cycle during our investigation period from July 2018 to June 2019 is cotton (Kharif season, monsoon) and wheat (Rabi season, inter-monsoon). The water allocation is realized with the Warabandi system (Narain, 2008) and applied to the plants by flood irrigation. While for the total LCC system and its larger irrigation subdivisions fairly precise canal supplies are known, on the field-scale only sparse data are available on irrigation operations and irrigation volumes (Ahmad et al., 2009). The long-term (1981–2019) average annual air temperature, precipitation and potential evaporation of the study site are 24.6°C, 540 mm and 2540 mm, respectively (Muñoz Sabater, 2019). The soil type is classified as sandy loam (locally termed Farida), which is the most abundant soil type in the LCC system (Awan & Ismaeel, 2014).

According to Köppen–Geiger, the climate in the Punjab region is generally classified as hot arid (Kottek et al., 2006), and only irrigation water allows intensive agriculture. Overall, this makes the Punjab region with the Indus Basin Irrigation System one of the largest closed irrigation areas with the world's second largest blue water footprint of 50 Gm^3 a^{-1} after Utter Pradesh (Ganges) and before California (Mekonnen & Hoekstra, 2011). The main irrigation water source for the Punjab is surface water from the Indus and its tributaries. However, measures against waterlogging (Bhutta & Smedema, 2007), steadily rising irrigation water demand, substantial transmission losses in the canal distribution system (Chaudhry, 2015), not demand-oriented water allocation (Basharat & Tariq, 2013), and large differences between up and downstream water availability (Kazmi et al., 2012) lead to an increasing exploitation of local groundwater resources (Habib, 2004). In addition to falling groundwater levels, the Punjab is strongly affected by increasing soil and groundwater salinization (Bhutta & Smedema, 2007), which is a quite typical phenomenon of irrigated agriculture in arid regions (Foster et al., 2018). In
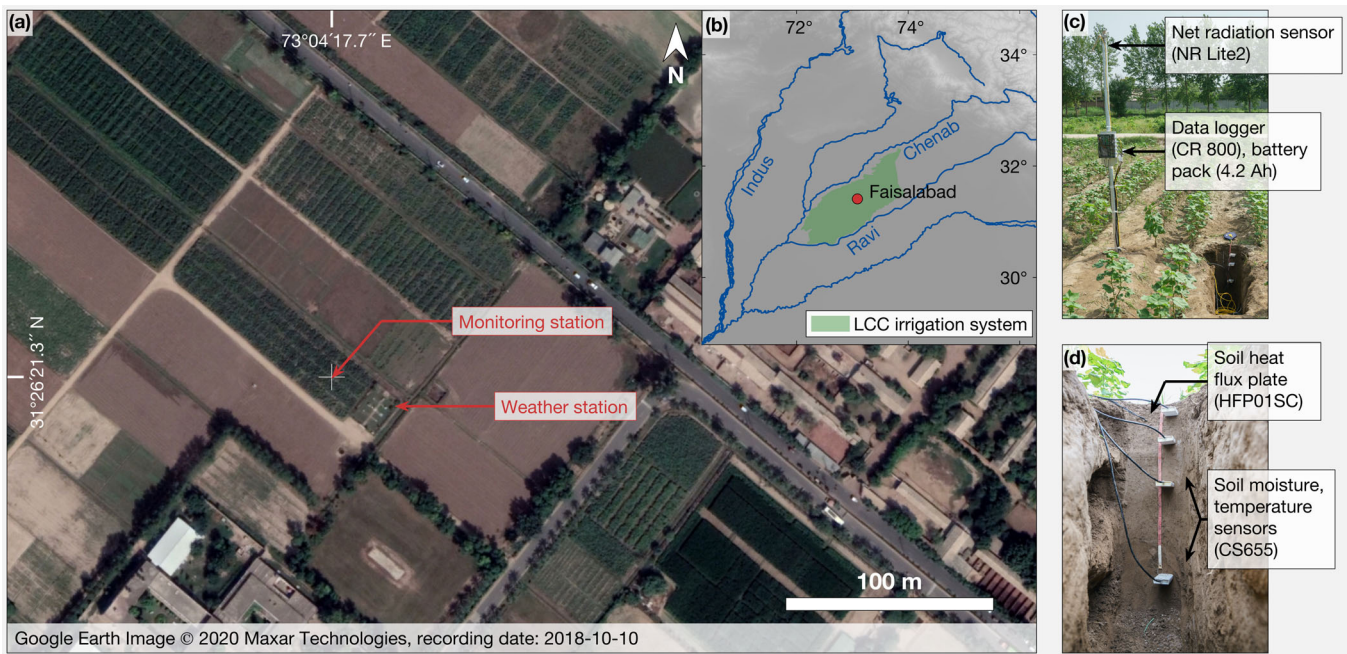
FIGURE 1 (a) True colour satellite image from 10 October 2018 of the test site. (b) Overview map with the Lower Chenab Canal (LCC) system. (c) Monitoring station on the test field with young cotton plants. (d) Subsurface part of the monitoring station with soil heat flux plate and four soil moisture and temperature sensors

order to counteract these trends and make agriculture in this region more sustainable, management adjustments are necessary, which require a quantification of the water balance components.

3 | MATERIALS AND METHODS

3.1 | Monitoring and soil sampling

A monitoring station was installed in July 2018 on a test field of the University of Agriculture Faisalabad (UAF) in Pakistan (Figure 1). The station is located at 73°04′17.7″N, 31°26″21.3″E and is equipped with the following devices:

1. one net radiometer (NR-Lite2, Kipp & Zonen), mounted at a height of 2.5 m to a vertical pipe;
2. one self-calibrating soil heat flux plate (HFP01SC, Hukseflux), installed in a depth of 8 cm below ground level (b.g.l.);
3. four soil moisture and temperature sensors (CS650, Campbell Scientific), installed in a depth of 10, 20, 40 and 80 cm b.g.l., respectively;
4. one data logger (CR800, Campbell Scientific), mounted to the vertical pipe of the net radiometer and set to a 1-min recording interval;
5. one 12 V battery with a capacity of 4.2 Ah.

This station was in operation from 3 July 2018 to 1 June 2019. Due to empty batteries or full memory storage the records show some gaps. The cumulative gap length is 51 days, and the number of full days with records is 281. This database is available via https://doi.pangaea.de/10.1594/PANGAEA.921389 (Schulz, 2020).

Additionally, routine weather data such as air temperature (minimum, maximum and mean), relative humidity, precipitation, class A pan evaporation, sun shine duration, and wind speed are available from a nearby (<100 m) weather station.

During the installation of the monitoring station, we took three undisturbed soil samples using 250 mL soil sample rings in depths of 10, 40 and 80 cm b.g.l., respectively. The samples were oven-dried at 105°C for 24 h and weighted to derive the bulk density. Subsequently, the three sub-samples per layer were combined and wet sieved with various mesh sizes to quantify the mass fractions for particle diameters larger than 63 μm. For particle diameters smaller than 63 μm, we carried out a sedimentation analysis. Results are given in the Table S1.

3.2 | Overview of data processing methodology

To estimate the water balance components ET_{act}, GWR, and water inflow we apply an approach, which comprises a series of data processing steps (Figure 2). First, we estimate reference crop evapotranspiration (ET_0) using energy balance data from our monitoring station and routine weather data. Subsequently, surface reflectance data from satellite images (Sentinel-2) are used to derive time-variable plant-specific information such as leaf area index (LAI), which then serves to partition ET_0 into energy limited evaporation (E_{max}) and transpiration (T_{max}). The next step is a first approximation of the inflow (sum of precipitation and irrigation) by inverting the soil water balance equation. Required changes in soil moisture storage are derived from interpolation and integration of the observed soil moisture data. To account for uncertainties, resulting from interpolation, a range of soil
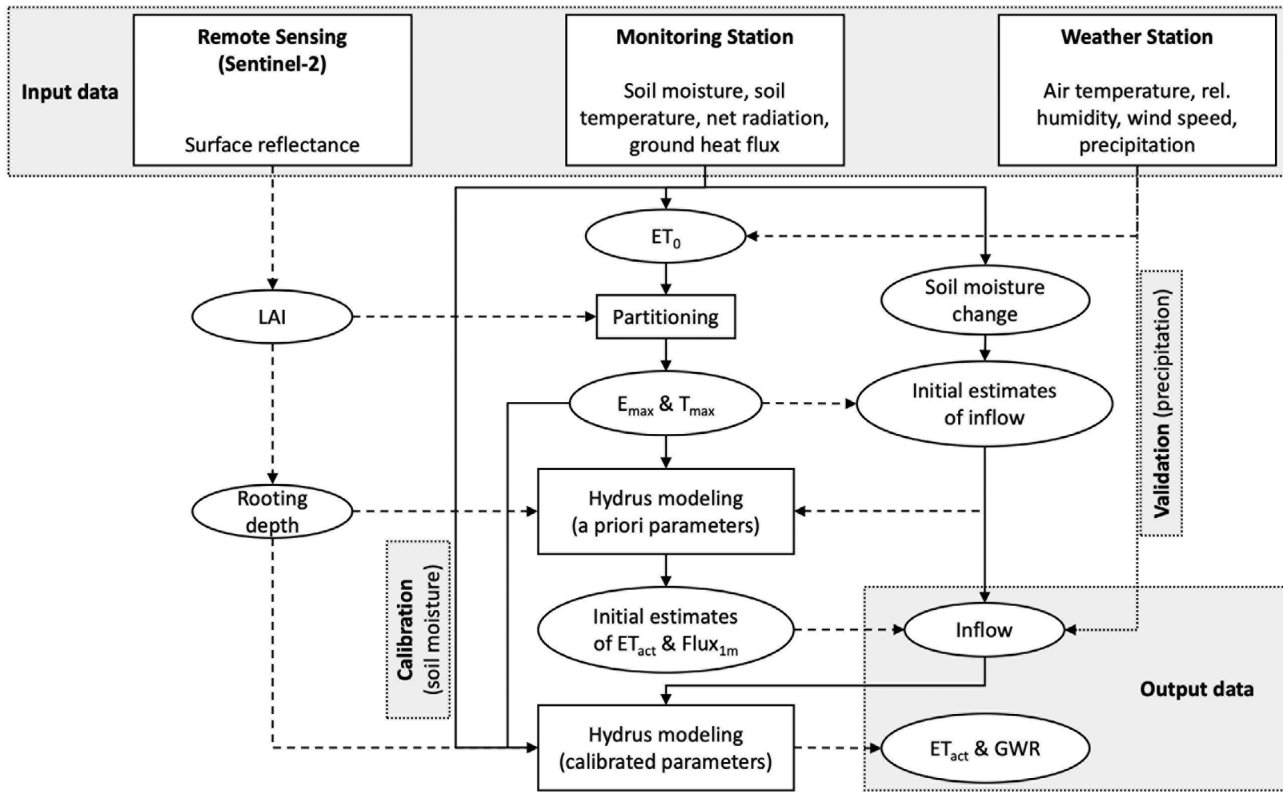
FIGURE 2 Overview of data processing methodology

moisture changes are calculated by applying different interpolation schemes. Moreover, at this stage, drainage is neglected and the sum of E_{max} and T_{max} serves as a first guess of ET_{act}.

Afterwards, we perform a first series of forward simulations of the water flow in the unsaturated zone and the root water uptake using Hydrus. The upper boundary conditions for this model are first approximations of the water inflow, E_{max}, and T_{max}. To further account for soil parameter uncertainties, we run simulations with a quite wide range of a priori estimates of van Genuchten parameters, derived from a soil texture analysis. This first modelling step yields a range of estimates for ET_{act} and drainage (flux at 1 m b.g.l.), which are then used to better estimate the inflow from the inverted soil water balance equation. The final step is to incorporate these improved inflow estimates into the model and calibrate the soil parameters by inverse modelling. Here, the observed soil moisture data form the reference figure for calibration. Forward simulations with calibrated soil parameters and improved inflow estimates result in final estimates for ET_{act} and GWR. A detailed description of all processing steps is given in the following sections.

3.3 | Evapotranspiration

3.3.1 | Radiation balance

The amount of energy, which is available for the latent heat (LE) and the sensible heat (H), is defined by the one-dimensional surface energy balance (Equation 1, Hartmann, 2016).

$$LE + H = Rn - G \tag{1}$$

While the net radiation (Rn) is directly measured by the net radiometer, the estimation of the ground heat flux (G) requires some computation. The heat flux, which we measure with our monitoring station, is the flux in a depth of 8 cm (G_{8cm}). To derive the ground heat flux, we need to account for a storage term (S_{heat}), which describes the change of heat stored in the layer above the heat flux plate (Equation 2).

$$G = G_{8cm} + S_{heat} \tag{2}$$

The storage term depends on the volumetric heat capacity of the moist soil (C_s) and is defined in Equation (3) (Hartmann, 2016).

$$S_{heat} = dT_s \cdot \frac{dz}{dt} \cdot C_s \text{ with } C_s = \rho_s \cdot c_s \cdot f_s + \rho_w \cdot c_w \cdot f_w \tag{3}$$

Estimates for the soil temperature change (dT_s) over the time period (dt) as well as the volume fraction of water (f_s) of the upper soil layer with a thickness (dz) of 8 cm base on records from the uppermost (10 cm b.g.l.) soil moisture and temperature sensor. The product of the soil density (ρ_s) and the volume fraction of soil (f_s) is the previously determined bulk density. The specific heat capacity of most dry mineral soils (c_s) and of water (c_w) are 837 and 4190 J kg^{-1} K^{-1}, respectively, and the density of water (ρ_w) is assumed to be 1.00 g cm^{-3} (Hanks, 1992).

3.3.2 | Leaf area index and rooting depth

Leaf area index (LAI) and rooting depth are plant characteristics, which are required to quantify transpiration, that is, LAI serves for partitioning of evapotranspiration (Allen et al., 1998) and rooting depth defines the soil depth from which plants can take up water (Feddes et al., 1976).

Leaf area indices (LAI) for our test site are estimated using red and near-infrared reflectance data. This approach was introduced by Clevers (1989) and bases on an empirically derived linear relationship (Equation 4) between LAI [$m^2\,m^{-2}$] and the weighted difference vegetation index (WDVI).

$$LAI = 0.109 \cdot WDVI - 0.3233 \qquad (4)$$

Furthermore, Clevers (1989) suggests to calculate the WDVI using red (R_{670}) and near-infrared (R_{870}) reflectance data of the plant canopy and the soil ($R_{670,soil}$ and $R_{870,soil}$), respectively (Equation 5).

$$WDVI = R_{870} - C \cdot R_{670} \text{ with } C = \frac{R_{870,soil}}{R_{670,soil}} \qquad (5)$$

Given the availability of high-resolution satellite data, Clevers et al. (2017) revisited this approach and proofed its usability with space-borne multispectral reflectance data from the Sentinel-2 satellite mission. An advantage of this approach, especially for small-scale applications such as in the presented case, is the relatively high spatial resolution of 10 m of the required spectral information, that is, band 4 (665 nm) and band 8 (842 nm).

For this study, 65 sets of satellite images are analysed, covering our monitoring period from 10 July 2018 to 1 June 2019. To allow for the further use of these scenes, the data are converted from top-of-atmosphere into top-of-canopy reflectance using the atmospheric correction procedure sen2cor (Louis et al., 2016). Afterwards, images with haze or clouds covering our test field are excluded. For the remaining images, reflectance values of band 4 and 8 are extracted from the pixel at the location of our monitoring station. To calculate the slope of the soil line (C in Equation 5) we use averages of the band values at the same location of images at times between cropping periods, that is, with bare soil.

Rooting depth (r_d) is assumed to be proportional to the soil cover fraction (SCF; Equation 6; Wongkaew et al., 2018).

$$\frac{r_d}{SCF} = constant \qquad (6)$$

The value for the constant in Equation (7) can be determined by dividing the maximum rooting depth by the maximum SCF. While maximum rooting depths are tabulated for various crop types in the FAO Irrigation and Drainage Paper No. 56 (Allen et al., 1998), SCF is calculated according to Equation (7) (Campbell & Norman, 1998).

$$SCF = 1 - e^{(-K_b \cdot LAI)} \qquad (7)$$

Plant-specific canopy extinction coefficients (K_b) are also available from Allen et al. (1998). The extinction coefficients for cotton and wheat are 0.65 and 0.55, and the maximum rooting depths are 1.35 m and 1.65 m, respectively.

3.3.3 | Energy-limited evapotranspiration

Estimates of energy-limited (soil) evaporation and energy-limited transpiration, that is, not limited by the availability of water, are derived from methods suggested in the FAO Irrigation and Drainage Paper No. 56 (Allen et al., 1998). Parts of these methods are slightly adapted to better meet the requirements of the numerical simulation tool Hydrus. First, reference crop evapotranspiration (ET_0) is calculated based on the FAO Penman–Monteith method, thoroughly described by Allen et al. (1998), using data from our monitoring station (Rn and G) and routine weather data from the nearby weather station. In order to separate ET_0 into a plant-specific and energy-limited transpiration and evaporation component, we applied the dual crop coefficient approach. Here, transpiration is calculated without considering limitations in soil water availability and thus, constitutes maximum possible transpiration (T_{max}), Equation (8).

$$T_{max} = ET_0 \cdot K_{cb} \qquad (8)$$

The basal crop coefficient (K_{cb}) characterizes the growth stage of the plant and can be derived from the time-variable LAI (Equation 9).

$$K_{cb} = K_{c\,min} + (K_{cb\,full} - K_{c\,min}) \cdot (1 - e^{-0.7 \cdot LAI}) \qquad (9)$$

$K_{c\,min}$ is the minimum crop coefficient for bare soil (K_c = 0.15) and $K_{cb\,full}$ is the plant-specific K_{cb} during the mid-season at peak plant height. $K_{cb\,full}$ for cotton and wheat are 1.15 and 1.1, respectively (Allen et al., 1998).

Evaporation from the soil (E) depends strongly on the growth stage of the plant, that is, the more of the soil surface is covered by plants, the lower the evaporation. In contrast to the previous calculation of transpiration, evaporation additionally bases on the availability of soil water for evaporation, described by the evaporation reduction coefficient (K_r, Equation 10). However, for further use in Hydrus we are only interested in the energy-limited (maximum possible) evaporation (E_{max}). Therefore, we set K_r to its maximum value of 1, which results in Equation (11).

$$E = ET_0 \cdot K_r \cdot (K_{c\,max} - K_{cb}) \qquad (10)$$

$$E_{max} = ET_0 \cdot (K_{c\,max} - K_{cb}) \qquad (11)$$

The maximum crop coefficient ($K_{c\,max}$) represents the upper limit for the actual evapotranspiration, considering the constraints of the available energy (Equation 12).

$$K_{c\,max} = \max\left(\left\{1.2 + [0.04 \cdot (u_2 - 2) - 0.004(RH_{min} - 45)] \cdot \left(\frac{h}{3}\right)^{0.3}\right\}, \{K_{cb} + 0.05\}\right) \qquad (12)$$

Wind speed at 2 m height (u_2) and daily minimum relative humidity (RH_{min}) are obtained from the nearby weather station. The mean plant heights during mid or late season stages (h) for cotton and wheat are 1.2 m and 1.0 m, respectively (Allen et al., 1998).

Crop coefficients and evapotranspiration rates are initially calculated on a daily basis. However, hourly values are required for the model. To downscale daily values to hourly values, daily rates of E_{max} and T_{max} are multiplied by the hourly relative diurnal variations of the theoretically maximum available energy for evapotranspiration (LE + H), exemplified for E_{max} in Equation (13) (indices 1–24 represent the hours of a day).

$$\begin{pmatrix} E_{max,\,1} \\ E_{max,2} \\ \vdots \\ E_{max,24} \end{pmatrix} = E_{max} \cdot \begin{pmatrix} LE_1 + H_1 \\ LE_2 + H_2 \\ \vdots \\ LE_{24} + H_{24} \end{pmatrix} \bigg/ \sum_{h=1}^{24} LE_h + H_h \qquad (13)$$

To allow a comparative analysis to the estimation of energy-limited evaporation and transpiration described above, which bases on energy balance data from our monitoring station and routine weather data from the nearby weather station, we apply two alternative methods. First, we followed the same procedure as described above, but for the estimation of ET_0 we use only data from the nearby weather station, that is, air temperature, relative humidity, wind speed and sunshine hours (Allen et al., 1998). Second, we calculate the theoretical maximum available energy for evapotranspiration (LE + H), using only data from our monitoring station, that is, Rn and G. Here, the temperature-dependent latent heat of vaporization was calculated using the temperature recordings of the upper CS650 sensor and an approach proposed by Henderson-Sellers (1984). These two alternative methods are evaluated by comparing them to the previously presented approach and may serve as an alternative when not all required data are available.

3.4 | First approximation of inflow

For days with observed positive changes in soil water storage, we assume that either precipitation or irrigation must have taken place. For these days we calculate the amount of water inflow (sum of irrigation and precipitation) using the water balance of the first meter of the unsaturated zone (Equation 14).

$$Inflow = dS_{1m} + flux_{1m} + ET_{act} \qquad (14)$$

Daily changes of soil moisture storage in the upper 1 m (dS_{1m}) result from the water volume stored at the end of the day (t) minus the water volume stored at the end of the previous day (t-1). To estimate these water volumes, first, temperature corrected (Campbell Scientific, 2018) measurements of volumetric water content (θ) at 10, 20, 40 and 80 cm b.g.l. are extrapolated, yielding continuous

values every 10 cm. Subsequently, extrapolated soil moistures are integrated over the first 1 m (dz, Equation 15).

$$dS_{1m} = \int_0^{1\,m\,b.g.l.} \theta_t(z)\,dz - \int_0^{1\,m\,b.g.l.} \theta_{t-1}(z)\,dz \qquad (15)$$

This approach introduces some uncertainty as the application of different extrapolation schemes result in different daily changes of soil moisture storage. To quantify this uncertainty, we run the extrapolation with the five standard interpolation methods that are available in Matlab 2020a: 'linear', 'nearest', 'makina', 'pchip' and 'spline'. The lowest and the highest estimate for dS_{1m} constitute the lower and upper bound of the uncertainty range, respectively.

Since we do not know too much about the variables $flux_{1m}$ (flux at 1 m depth, previously referred to as drainage) and ET_{act}, for now, we apply the initial assumption $flux_{1m} = 0$ and $ET_{act} = E_{max} + T_{max}$. This step serves only for a first estimation of the inflow and in second step better estimates of $flux_{1m}$ and ET_{act} will be available. Nevertheless, we expect that this assumption is not too far from reality. On a daily basis, the expected $flux_{1m}$ is quite low compared to the relatively large, periodically applied inflow quantities that are common in flood irrigation. Moreover, irrigation contributes to a constant water supply for evaporation, which allows the assumption that evapotranspiration is mostly energy-limited.

3.5 | Numerical modelling

Modelling of water flow and root water uptake are performed with the numerical simulation tool Hydrus (Šimůnek et al., 2008). Our model represents a one-dimensional vertical soil profile, divided into three layers of 0–15 cm b.g.l., 15–60 cm b.g.l. and 60–200 cm b.g.l., and it covers a time period from 16 August 2018 to 4 May 04. The vertical spatial resolution, i.e. the distance between two neighbouring nodes, is 1 cm and the temporal resolution is 1 h. Time variable energy-limited evaporation and transpiration, and water inflow (sum of irrigation and precipitation) constitute the upper boundary. As our simulated soil profile is quite deep (2 m b.g.l.) and still far away from the groundwater table (approximately at 10 m b.g.l.), we do not expect a significant capillary rise from deeper layers into our profile and thus, set the lower boundary to free drainage. The hydraulic properties of the soil are described by the van Genuchten–Mualem model (van Genuchten, 1980). To account for temperature changes and their effects on the soil hydraulic properties, we also simulate the heat flow and activate the temperature correction function in Hydrus. Thermal conductivity parameters of loam are derived from the internal database of Hydrus (Chung & Horton, 1987). The time-variable upper and lower Dirichlet boundary conditions of the heat flow model are linearly extrapolated temperatures of the soil surface and 2 m b.g.l., respectively. Parallel to the flow modelling, root water uptake is simulated using the Feddes model (Feddes et al., 1976). Parameter of the Feddes model for cotton and wheat base on values provided by

Taylor and Ashcroft (1972), cited in Forkutsa et al. (2009) and Wesseling (1991), respectively.

3.5.1 | Final estimation of inflow

Final estimates of inflow are derived from a first model application. The van Genuchten parameters (VGP) and the saturated hydraulic conductivity (K_s) of the model are not yet calibrated and only a priori estimates based on the particle size distribution and the bulk density are available. These estimations are predicted by pedotransfer functions implemented in the Rosetta model (Schaap et al., 2001; Zhang & Schaap, 2017). This is an elegant and frequently used approach. However, due to its empirical nature (pedotransfer functions are derived from a neural network analysis of a soil database), it is associated with uncertainties that are quantified with the standard deviations (σ) resulting from a bootstrap-resampling method (Zhang & Schaap, 2017). In this study, except for the saturated water content (θ_s), the range of the a priori estimation of the hydraulic parameters is defined as their mean predicted value $\pm 2 \cdots \sigma$. Due to intense irrigation, that is, high availability of water, we assume that the highest observed volumetric water content is a good estimate for θ_s.

Now we perform a series of forward simulations with all possible parameter configurations for all three soil layers and the five initial estimates of the inflow. The resulting sets of simulations of flux$_{1m}$ and ET$_{act}$ are used to improve the calculation of the inflow (Equation 14). Maximum and minimum estimates represent the uncertainty range of the inflow.

3.5.2 | Parameter optimization

With an estimation of the inflow boundary condition and a quantification of its uncertainty, we can carry out an optimization of the hydraulic parameters. For this purpose, we apply an inverse modelling approach using the PEST (Model-Independent Parameter Estimation and Uncertainty Analysis) tool (Doherty, 2015). Here we employ the global optimization tool CMA-ES (Covariance Matrix Adaptation Evolution Strategy) to minimize the objective function, that is, the sum of squared residuals of simulated and observed volumetric soil moisture (Hansen, 2006). In analogy to the estimation of the inflow uncertainty, we use the mean predicted value $\pm 2 \cdots \sigma$ from the Rosetta model as the parameter range for the VGPs and K_s during optimization. θ_s is an exception here as well. This parameter is kept constant on its a priori estimated value, that is, the highest observed volumetric water content. The optimization procedure is applied for the minimum, mean and maximum inflow estimations, resulting in three sets of calibrated hydraulic parameters.

4 | RESULTS AND DISCUSSION

4.1 | Evapotranspiration

4.1.1 | Radiation balance

The observed average energy flux at the surface (top of canopy or ground) of our test site is 119 and 0.2 W m^{-2} from net radiation (Rn) and ground heat flux (G), respectively (Figure 3a). With this, ground
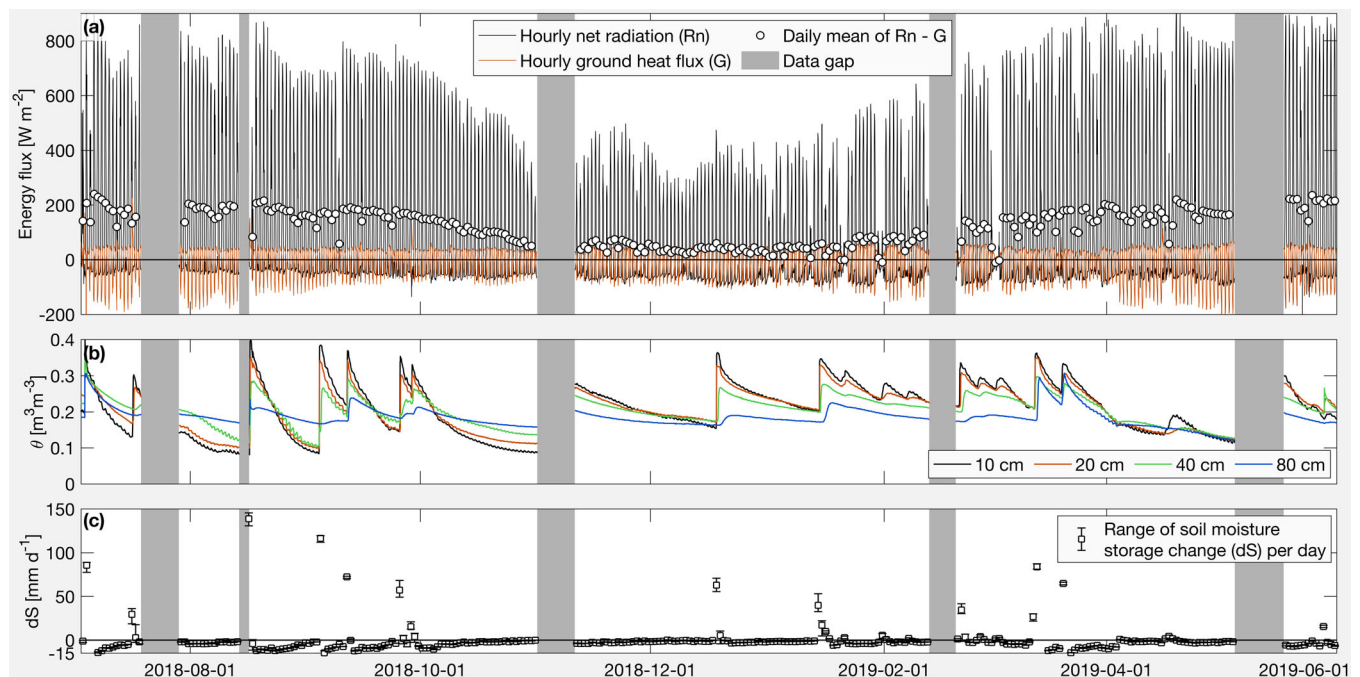

FIGURE 3 (a) Records of net radiation and ground heat flux. (b) Records of volumetric water content. (c) Daily changes in soil moisture storage

heat flux contributes on average less than 1% to the total energy budget (Rn-G). However, looking at the daily values, the share of ground heat flux ranges approximately between −50% and 10% with negative values referring to an energy flow from the soil into the atmosphere and positive values vice versa. The mean absolute value of the daily fraction is 16%. Typically, it is assumed that the magnitude of the ground heat flux in day periods is very small and may therefore be neglected (Allen et al., 1998). However, this seems to be too much of a simplification for our system. A possible explanation can be found in the specific conditions for our test site. Due to the intensive irrigation, our soil is almost always moist, which results in a rather high heat capacity of our soil, since the specific heat capacity of water is more than four times higher than that of mineral soil (Hanks, 1992). Combined with a high but variable energy input due to climatic conditions, this can result in a high energy storage in the soil, which does not allow for quick heat equalization.

4.1.2 | Leaf area index and rooting depth

The basis for estimating LAI and rooting depth is the canopy or soil reflection data from the Sentinel 2 satellite mission. After sorting out the images with haze or cloud cover over our test field, 11 images for cotton, 9 images for wheat and 7 images for bare soil remained for our observation period. From the images showing bare soil, we calculated a value of 1.39 for the slope of the soil line (C in Equation 5). For both cotton and wheat, the temporal development of the LAI clearly shows the different growth stages from early plant development to harvest (Figure 4a). Observed values for cotton and wheat range from 0.1 to 1.7 and from 0.4 to 3.2, respectively. The rooting depth depends on the constant canopy extinction coefficients and the time-dependent LAI and thus shows a similar temporal pattern as the LAI.

4.1.3 | Energy-limited evapotranspiration

Energy-limited evapotranspiration ($E_{max} + T_{max}$) show pronounced inter-annual variabilities with higher rates during the hot summer months (up to almost 10 mm day^{-1}) and significantly lower rates during the temperate winter months (Figure 4b). The partitioning of evapotranspiration is based on the dual crop coefficient concept. Like the rooting depth, crop coefficients highly depend on the LAI. The more photosynthetically active leaves the plant has, the larger the basal crop coefficient (K_{cb}) and thus the higher the share of transpiration. In case of bare soil, K_{cb} is zero and only evaporation takes place. On average, the sum of K_{cb} and the share for E_{max} ($K_{c\ max} - K_{cb}$) is 1.11 (Figure 4a). This means that the energy-limited evapotranspiration of our test site is 11% higher than the reference crop evapotranspiration (ET_0), that is, ET_{act} of short, green and well-watered grass.

This is quite an important observation, as it is not uncommon to use ET_0 as so called potential evapotranspiration, which then defines the upper limit for actual evapotranspiration in Hydrus (Šimůnek et al., 2013). In most cases this is a well working assumption. However, in cases with a high energy input, tall crops and almost permanent excess of water, for example, through irrigation, actual evapotranspiration may easily exceed ET_0 (Kirkham, 2014; Rosenberg, 1974).

Noteworthy findings also result from the comparison of the different possibilities to estimate evapotranspiration. For our study, we used energy-limited evaporation (E_{max}) and transpiration (T_{max}) estimates derived from methods proposed in the FAO Irrigation and Drainage Paper No. 56 (Allen et al., 1998) using energy balance data, that is, Rn and G, from our monitoring station as well as routine weather data from the nearby weather station. Additionally, we estimated the energy-limited evapotranspiration with two alternative methods. One of them uses only energy balance data from our
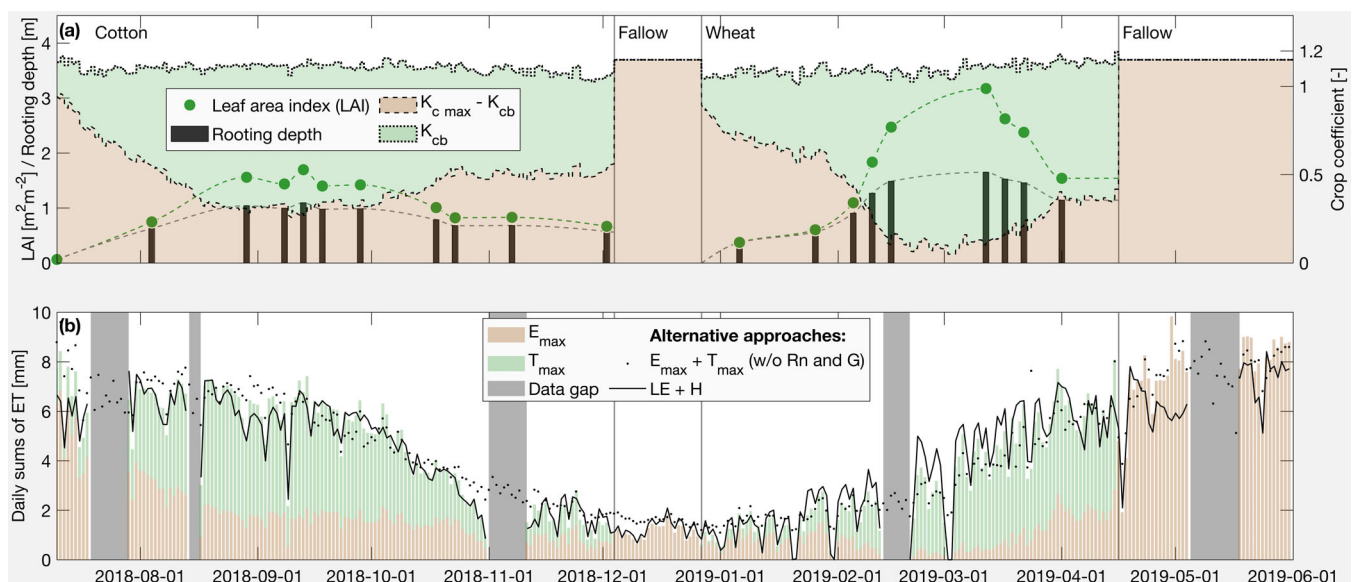

FIGURE 4 (a) Temporal evolution of LAI, rooting depth and crop coefficient components. (b) Daily sums of energy-limited evaporation (E_{max}) and transpiration (T_{max}), and alternative estimates for energy limited evapotranspiration estimates

monitoring station and the other one uses only routine weather data. Results from the two alternative methods show a similar pattern as our approach (Figure 4b). The root mean square error (RMSE) of the FAO approach using only routine weather data and the approach using only energy balance data compared to the FAO approach based on both data sets are 0.73 mm and 0.69 mm, respectively. While the first mentioned alternative seems to slightly overestimate the energy-limited ET (mean error of +0.23 mm), the energy balance approach shows on average almost no difference (−0.04 mm). At first, the even better performance of the energy balance approach is somewhat surprising, as it neglects any energy loss or input through sensible heat flux (H). However, the special conditions of our study area, that is, almost constantly well-irrigated soil and relatively high temperatures, associated with low advection and low Bowen ratios, may explain this finding (McMahon et al., 2013; Priestley & Taylor, 1972). In this regard, it should also be noted that the deviation of LE + H related to the energy-limited ET increases during the first half of the last fallow period when the soil dries out (compare Figure 3b and 4b). This supports the previously given explanation and likewise shows the limited validity of this alternative approach. Nevertheless, under the given conditions, that is, irrigated agriculture in a semi-arid environment, LE + H could be used as a first estimate for the energy-limited ET. This approach is quite attractive because of its simplicity. It does not require any assumptions for the FAO Penman–Monteith method, nor is it necessary to compute crop coefficients.

4.2 | First approximation of inflow

Daily soil moisture changes and energy limited evapotranspiration estimates constitute the base for the first approximation of inflow. Interpolation and subsequent integration of the observed soil moisture data (Figure 3b) yield daily changes in soil moisture storage (Figure 3c). Abrupt positive changes in soil moisture result either from precipitation or irrigation events and range from a few millimetres to almost 150 mm per day. More frequent, but less pronounced, are negative values of soil moisture storage changes representing water loss due to evapotranspiration and deep percolation. Here the maximum absolute rate is about 18 mm per day. The range of values resulting from the application of different interpolation schemes represents the uncertainty range.

Calculated first approximations of the daily inflow amounts for the different interpolation schemes are given in the Table S2. Estimates for single inflow events show differences of up 14 mm and their relative cumulative uncertainty range is 9.5%.

4.3 | Model results

4.3.1 | Final estimation of inflow

To improve the estimation of inflow, in addition to soil moisture change in the first meter (dS_{1m}), estimates of ET_{act} and flux at 1 m

depth (flux$_{1m}$) are required. These values and their uncertainties are derived from a series of forward simulations (Figure 5a). For this, all possible combinations of the different initial inflow estimates, which are based on the different estimates of the soil moisture storage changes, and the a priori van Genuchten parameters (VGP) are used (Figure 5b). The basis for the a priori parameter estimates is the grain size fractions and bulk densities of the three soil layers. These values and the resulting VGP are given in the Table S1 and S3, respectively. Not surprisingly, the derived initial set of ET_{act} and flux$_{1m}$ estimates show a rather wide range (Figure 5a). During the modelling period from16 August 2018 to 4 May 2019, the mean initial ET_{act} and the mean initial flux$_{1m}$ are 3.5 and 0.8 mm day^{-1} with a relative uncertainty range of 64% and 246%, respectively. At first glance, these uncertainties seem to be quite large. However, these values are only used for inflow estimation, and compared to the relatively large soil moisture changes of up to almost 150 mm day^{-1} this first impression is somewhat relativized. Finally, Equation (14) is applied to calculate three inflow time series using the mean, minimum and maximum values of dS, initial ET_{act}, and initial flux$_{1m}$, respectively. The final inflow estimates range from small events of only a few millimetres up to events of more than 150 mm (Table S5, Figure 6).

Comparing the uncertainty range of the first approximation of inflow (introduced by the application of different interpolation schemes) and the final inflow estimates (based on both, interpolation and a priori soil parameter uncertainty) provides information about the sensitivity of the different interpolation methods and soil parameters. While the first approximation of the inflow shows a mean relative uncertainty of 9.5%, it increases to 23.8% for the final estimates (compare Table S2 and S5). This suggests that both sources of uncertainty are quite similarly sensitive.

4.3.2 | Parameter optimization

The second stage is the VGP optimization. With the exception of the saturated water content (θ_s), the upper and lower parameter limits for optimization are defined by the a priori parameter range (Figure 5b). θ_s of layer 1 is kept constant at the highest observed water content (θ_{obs}) of 40.6% recorded by the sensor at 10 cm b.g.l. θ_s of layer 2 is set to 35.0%, the highest observed values of the sensor at 20 cm b.g.l. Due to comparable soil properties of layer 2 and layer 3 and the difficulty of reaching saturation at greater depth, we also assume a value of 35.0% for θ_s of layer 3. The calibration procedure is performed separately for the minimum, mean and maximum inflow estimates. This results in three different optimized parameter sets, representing the range of the posterior parameter uncertainties (Figure 5b). Values for the optimized VGP are given in the Table S4. The simulated volumetric water contents with the best fitting parameter sets of the three inflow cases are quite similar and show fairly satisfactory fits to the observed values (Figure 5c). The goodness-of-fit, expressed as root mean squared error, of the minimum, mean and maximum inflow case is 2.3%, 2.2% and 2.2% respectively.
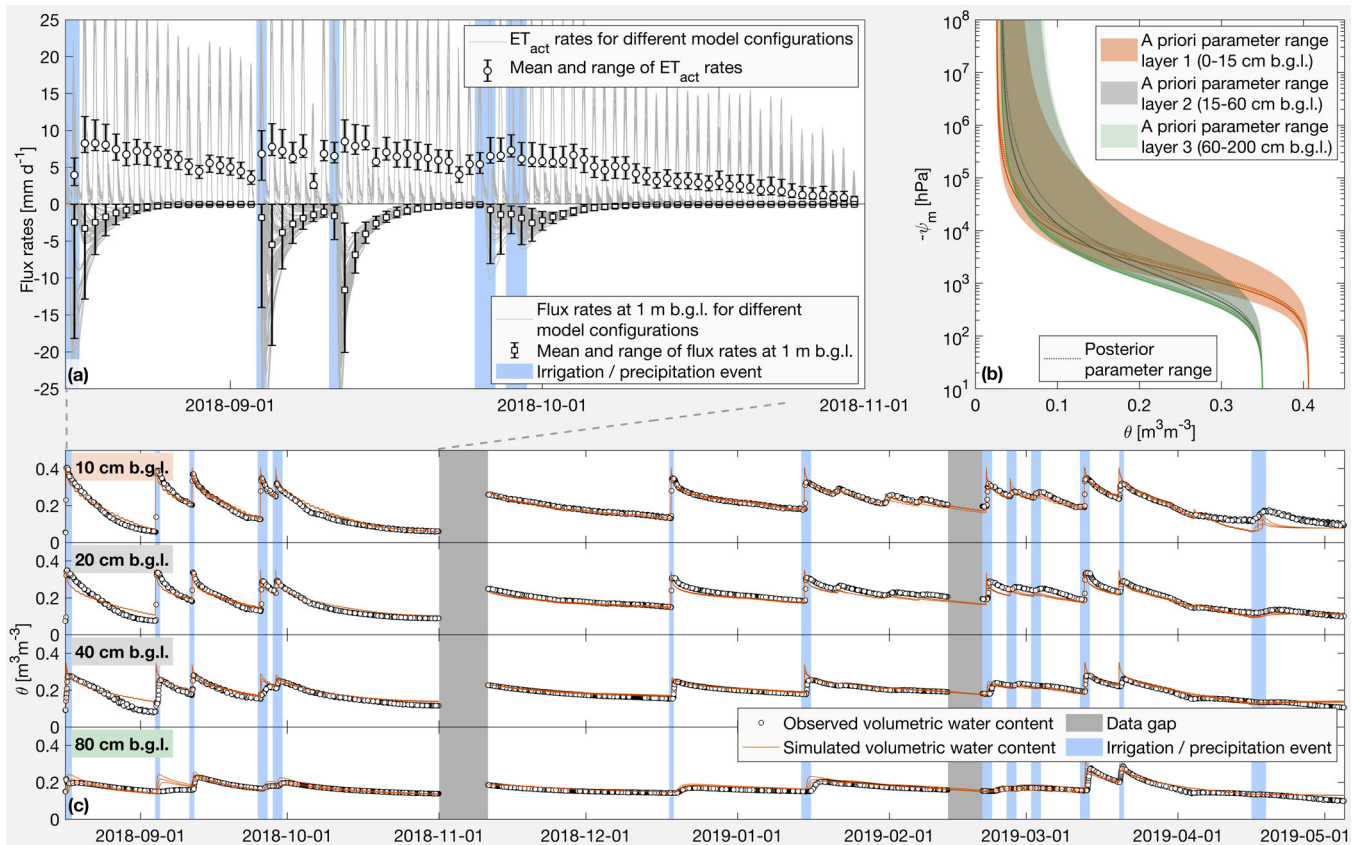
FIGURE 5 (a) Exemplary data sets from the first modelling stage with first estimates of actual evapotranspiration and flux at 1 m b.g.l. (b) Soil water retention curves representing the a priori and posterior (optimized) van Genuchten parameter ranges of the three soil layers. (c) Simulated and observed volumetric water contents of the four sensor positions for the entire modelling period from 16 August 2018 to 4 May 2019
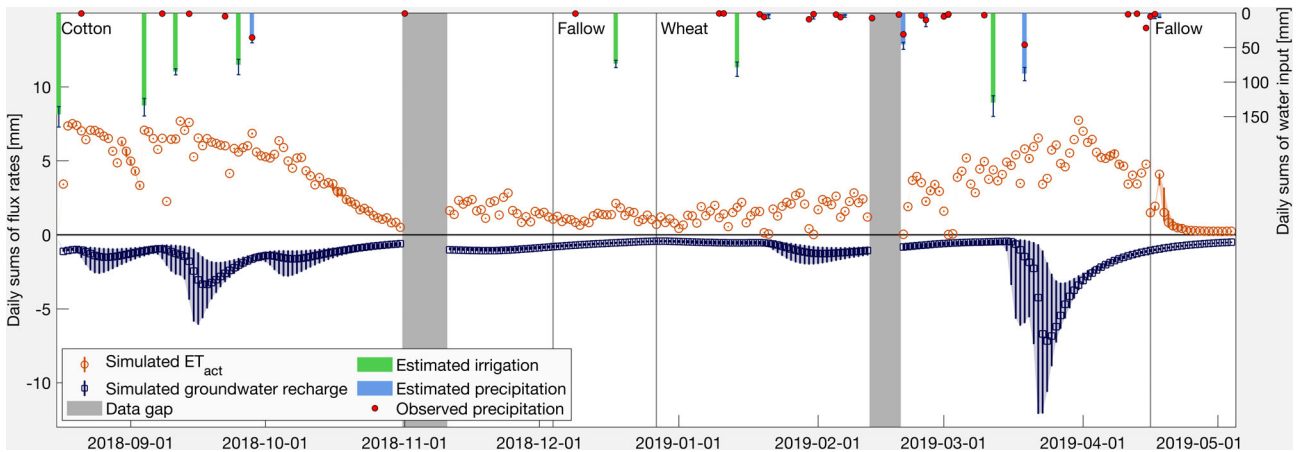

FIGURE 6 Final inflow estimates and simulation results of actual evapotranspiration and groundwater recharge for the period from 16 August 2018 to 4 May 2019

4.3.3 | Prognostic runs

Finally, the model is applied in a forward simulation using the three different optimized parameter sets to estimate ET_{act} and the flux in 2 m ($flux_{2m}$), which constitutes the bottom flux of our model, and their associated uncertainties (Figure 6). The simulation with the

parameters, resulting from the optimization using the mean inflow estimate, yields 769 mm and 297 mm of cumulative ET_{act} and $flux_{2m}$, respectively. These outflow components are balanced by a cumulative inflow of 946 mm. The difference of 120 mm results mainly from an unrecorded irrigation event during the first data gap and a soil moisture storage change over the modelling period. While the ET_{act} shows

TABLE 1 Seasonal sums of simulated and observed water balance components

| Period | Crop | | Simulated | | | | Observed |
			ETact [mm]	GWR [mm]	Irrigation [mm]	Precipitation [mm]	Precipitation [mm]
16 August 2018 to 4 December 2018	Cotton	min	407.3	94.3	406.8	32.2	42.3
		mean	411.6	132.0	440.2	36.7	
		max	413.2	186.5	493.3	43.1	
4 December 2018 to 27 December 2018	Fallow	min	27.8	12.3	68.5	0.0	0.7
		mean	27.9	13.4	73.4	0.0	
		max	28.0	14.4	79.0	0.0	
27 December 2018 to 17 April 2019	Wheat	min	308.7	90.4	190.9	141.4	154.1
		mean	309.8	138.9	208.4	168.3	
		max	310.6	209.5	241.7	205.4	
17 April 2019 to 4 May 2019	Fallow	min	9.4	11.9	0.0	9.7	6.6
		mean	12.7	12.2	0.0	12.5	
		max	16.9	12.9	0.0	14.6	
16 August 2018 to 4 May 2019	Total	min	753.2	208.9	666.2	183.3	203.7
		mean	762.1	296.5	722.0	217.5	
		max	768.6	423.3	814.1	263.1	

only a small uncertainty range of 2.1%, the uncertainties of the $flux_{2m}$ estimates are significantly larger with a range of about 72%. This is not a surprising result. Our test site is always very well-watered and consequently ET_{act} is likely most of the time as high as the sum of E_{max} and T_{max} (Figure 6). In order to fulfil continuity in the water balance, the uncertainty of the inflow is therefore mainly related to the uncertainty of $flux_{2m}$. Daily sums of simulated values of inflow, ET_{act} and $flux_{2m}$, as well as their associated uncertainty ranges are given in the Table S5.

Due to a rather deep groundwater table of about 10 m b.g.l., a maximum rooting depth of 1.65 m and almost always well-watered conditions, one can expect a depth of the zero-flux plane of not more than 2 m b.g.l. Also, simulation results, that is, fluxes at various observation points, suggest a maximum depth of the ZFP of 1.47 m b.g.l. during our modelling period. Consequently, the flow direction at 2 m depth is always downward and the flux at 2 m depth ($flux_{2m}$) can be considered as groundwater recharge.

4.3.4 | Comparison of results with observed data

From the nearby weather station, daily precipitation amounts are available for our modelling period. These data are used to identify precipitation events in the simulated inflow time series, that is, inflow events that occur during a day or the following day when precipitation is recorded are attributed to precipitation. Thus, a comparison between measured and simulated precipitation is enabled. Generally, the measured precipitation pattern matches well with the one we estimated from the water balance. Except for a few small precipitation events (<5 mm) all precipitation events could be captured (Figure 6).

The reason for not detecting these small events is that low precipitation can be balanced out by evaporation during the day, that is, no positive change in daily soil moisture storage is observed. Nevertheless, the sums of the measured precipitation are within the error range of those simulated during cotton and wheat cultivation (Table 1). The deviation of simulated (mean) and observed precipitation over the total simulation period is 7% (14 mm).

During our modelling period, mean simulated precipitation might account for only 23% of the total inflow, while irrigation accounts for 77%, illustrating the rather large blue water footprint of cotton and wheat production in the region. Similar values are reported by Ahmad et al. (2002), who analysed the water balance of a cotton-wheat system of a comparable test field near Faisalabad from May 2000 to April 2001. For this period, they have measured a total precipitation and irrigation amount of 290 mm (26%) and 844 mm (74%), respectively.

5 | CONCLUSION

This study presents a method for estimating water balance components with moderate measurement efforts. We focus on the specific requirements of irrigated agriculture in semi-arid and arid environments. A particular aspect is that we do not need measurements of irrigation nor precipitation quantities to establish the water balance. This is quite useful as many irrigated areas lack the basic knowledge of these inflows. The final estimations of the actual evapotranspiration and groundwater recharge base on simulations with the numerical model Hydrus. This is also beneficial since models have predictive power and simulations could be performed to test different management scenarios, for example, different irrigation practices or crop cycles.

Although the presented method of the inflow estimation could also be applied to solely rainfed systems, it can be reasonably assumed that precipitation can be measured more simply and with much lower uncertainties, for example, with a rain gauge. However, it is different for irrigation. Theoretically, measurements are not complicated here either (simple flow meters would often be sufficient), but they would be needed for each field separately and farmers would have to keep accurate records. Moreover, irrigation water distribution over the field can vary considerably. This can lead to uncertainties if only one specific point is to be examined, as it is common, for example, in one-dimensional process analysis. Finally, the decision whether the presented approach is suitable depends on the research question and the available data. In this context, the two alternative methods for estimating energy limited evapotranspiration are also worth mentioning. If an accurate determination of evapotranspiration is not the primary goal, but only an estimation of irrigation or groundwater recharge, one of the presented alternatives can also be applied. They require less data and the differences between the methods are quite small compared to irrigation amounts.

Moreover, this study could show some shortcomings in frequently applied assumptions such as using ET_0 as the upper limit for actual evapotranspiration or neglecting the ground heat flux in the energy balance. For most cases these assumptions might work and constitute valid simplifications. However, for irrigated agricultural systems with a high but variable energy input, as common in arid regions, they seem to be too much of a simplification and should be avoided.

For our study area, but also for other irrigation systems in arid environments, the complex interplay of different aspects such as waterlogging and salinity control, preservation of drinking water resources and reduction of the blue water footprint while ensuring agricultural productivity requires finely tuned management. A profound knowledge of the hydrological processes and a reliable quantification of the water balance components are essential for this.

DATA AVAILABILITY STATEMENT

This database is available via https://doi.pangaea.de/10.1594/PAN-GAEA.921389 (Schulz, 2020).

ORCID

Stephan Schulz https://orcid.org/0000-0001-7060-7690
Juan Carlos Richard-Cerda https://orcid.org/0000-0001-9020-2973

REFERENCES

Ahmad, M.-D., Bastiaanssen, W. G. M., & Feddes, R. A. (2002). Sustainable use of groundwater for irrigation: A numerical analysis of the subsoil water fluxes. *Irrigation and Drainage*, 51(3), 227–241. https://doi.org/10.1002/ird.59

Ahmad, M. D., Turral, H., & Nazeer, A. (2009). Diagnosing irrigation performance and water productivity through satellite remote sensing and secondary data in a large irrigation system of Pakistan. *Agricultural Water Management*, 96(4), 551–564. https://doi.org/10.1016/j.agwat.2008.09.017

Allen, R. G., Pereira, L. S., Howell, T. A., & Jensen, M. E. (2011). Evapotranspiration information reporting: I. Factors governing measurement accuracy. *Agricultural Water Management*, 98(6), 899–920. https://doi.org/10.1016/j.agwat.2010.12.015

Allen, R. G., Pereira, L. S., Raes, D., & Smith, M. (1998). FAO Irrigation and Drainage Paper No. 56: Crop Evapotranspiration. Rome. Retrieved from http://www.fao.org/3/X0490E/X0490E00.htm

Awan, U. K., & Ismaeel, A. (2014). A new technique to map groundwater recharge in irrigated areas using a SWAT model under changing climate. *Journal of Hydrology*, 519, 1368–1382. https://doi.org/10.1016/j.jhydrol.2014.08.049

Basharat, M., & Tariq, A.-R. (2013). Spatial climate variability and its impact on irrigated hydrology in a canal command. *Arabian Journal for Science and Engineering*, 38(3), 507–522. https://doi.org/10.1007/s13369-012-0336-9

Becker, R., Koppa, A., Schulz, S., Usman, M., aus der Beek, T., & Schüth, C. (2019). Spatially distributed model calibration of a highly managed hydrological system using remote sensing-derived ET data. *Journal of Hydrology*, 577(123944), 123944. https://doi.org/10.1016/j.jhydrol.2019.123944

Bhutta, M. N., & Smedema, L. K. (2007). One hundred years of waterlogging and salinity control in the Indus valley, Pakistan: A historical review. *Irrigation and Drainage*, 56(S1), S81–S90. https://doi.org/10.1002/ird.333

Brocca, L., Ciabatta, L., Massari, C., Moramarco, T., Hahn, S., Hasenauer, S., Kidd, R., Dorigo, W., Wagner, W., & Levizzani, V. (2014). Soil as a natural rain gauge: Estimating global rainfall from satellite soil moisture data. *Journal of Geophysical Research: Atmospheres*, 119(9), 5128–5141. https://doi.org/10.1002/2014JD021489

Brocca, L., Massari, C., Ciabatta, L., Moramarco, T., Penna, D., Zuecco, G., Pianezzola, L., Borga, M., Matgen, P., & Martínez-Fernández, J. (2015). Rainfall estimation from in situ soil moisture observations at several sites in Europe: An evaluation of the SM2RAIN algorithm. *Journal of Hydrology and Hydromechanics*, 63(3), 201–209. https://doi.org/10.1515/johh-2015-0016

Brocca, L., Moramarco, T., Melone, F., & Wagner, W. (2013). A new method for rainfall estimation through soil moisture observations. *Geophysical Research Letters*, 40(5), 853–858. https://doi.org/10.1002/grl.50173

Brocca, L., Tarpanelli, A., Filippucci, P., Dorigo, W., Zaussinger, F., Gruber, A., & Fernández-Prieto, D. (2018). How much water is used for irrigation? A new approach exploiting coarse resolution satellite soil moisture products. *International Journal of Applied Earth Observation and Geoinformation*, 73, 752–766. https://doi.org/10.1016/j.jag.2018.08.023

Campbell, G. S., & Norman, J. M. (1998). *An introduction to environmental biophysics*. Springer: New York, NY.

Campbell Scientific. (2018). Instruction manual CS650 and CS655 water content Reflectometers: 58.

Chaudhry, S. A. (2015). Pakistan's Indus Basin water strategy: Past, present and future. In R. Amjad & S. J. Burki (Eds.), *Pakistan—moving the economy forward* (pp. 198–223). Delhi: Cambridge University Press.

Chung, S.-O., & Horton, R. (1987). Soil heat and water flow with a partial surface mulch. *Water Resources Research*, 23(12), 2175–2186. https://doi.org/10.1029/WR023i012p02175

Clevers, J. (1989). Application of a weighted infrared-red vegetation index for estimating leaf area index by correcting for soil moisture. *Remote Sensing of Environment*, 29(1), 25–37. https://doi.org/10.1016/0034-4257(89)90076-X

Clevers, J., Kooistra, L., & van den Brande, M. (2017). Using Sentinel-2 data for retrieving LAI and leaf and canopy chlorophyll content of a potato crop. *Remote Sensing*, 9(5), 405. https://doi.org/10.3390/rs9050405

Dari, J., Brocca, L., Quintana-Seguí, P., Escorihuela, M. J., Stefan, V., & Morbidelli, R. (2020). Exploiting high-resolution remote sensing soil moisture to estimate irrigation water amounts over a Mediterranean region. *Remote Sensing*, 12(16), 2593. https://doi.org/10.3390/rs12162593

Doherty, J. (2015). *Calibration and uncertainty analysis for complex environmental models*. Watermark Numerical Computing: Brisbane.

Feddes, R. A., Kowalik, P., Kolinska-Malinka, K., & Zaradny, H. (1976). Simulation of field water uptake by plants using a soil water dependent root extraction function. *Journal of Hydrology*, 31(1–2), 13–26. https://doi.org/10.1016/0022-1694(76)90017-2

Filippucci, P., Tarpanelli, A., Massari, C., Serafini, A., Strati, V., Alberi, M., Raptis, K. G. C., Mantovani, F., & Brocca, L. (2020). Soil moisture as a potential variable for tracking and quantifying irrigation: A case study with proximal gamma-ray spectroscopy data. *Advances in Water Resources*, 136, 103502. https://doi.org/10.1016/j.advwatres.2019.103502

Forkutsa, I., Sommer, R., Shirokova, Y. I., Lamers, J. P. A., Kienzler, K., Tischbein, B., Martius, C., & Vlek, P. L. G. (2009). Modeling irrigated cotton with shallow groundwater in the Aral Sea Basin of Uzbekistan: I. Water dynamics. *Irrigation Science*, 27(4), 331–346. https://doi.org/10.1007/s00271-009-0148-1

Foster, S., Pulido-Bosch, A., Vallejos, Á., Molina, L., Llop, A., & MacDonald, A. M. (2018). Impact of irrigated agriculture on groundwater-recharge salinity: A major sustainability concern in semiarid regions. *Hydrogeology Journal*, 26(8), 2781–2791. https://doi.org/10.1007/s10040-018-1830-2

Fraga, I., Cea, L., & Puertas, J. (2019). Effect of rainfall uncertainty on the performance of physically based rainfall-runoff models. *Hydrological Processes*, 33(1), 160–173. https://doi.org/10.1002/hyp.13319

van Genuchten, M. T. (1980). A closed-form equation for predicting the hydraulic conductivity of unsaturated soils. *Soil Science Society of America Journal*, 44(5), 892–898. https://doi.org/10.2136/sssaj1980.03615995004400050002x

Habib Z. (2004). Scope for reallocation of river waters for agriculture in the Indus Basin. École nationale du génie rural, des eaux et des forêts.

Hanks, R. J. (1992). *Applied soil physics*. Springer: New York, NY.

Hansen, N. (2006). The CMA evolution strategy: A comparing review. In J. A. Lozano, P. Larrañaga, I. Inza, & E. Bengoetxea (Eds.), *Towards a new evolutionary computation* (pp. 75–102). Berlin: Springer Berlin Heidelberg. https://doi.org/10.1007/3-540-32494-1_4

Hartmann, D. L. (2016). *Global physical climatology*. Amsterdam: Elsevier Science.

Healy, R. W. (2010). *Estimating groundwater recharge*. New York: Cambridge University Press.

Henderson-Sellers, B. (1984). A new formula for latent heat of vaporization of water as a function of temperature. *Quarterly Journal of the Royal Meteorological Society*, 110(466), 1186–1190. https://doi.org/10.1002/qj.49711046626

Kazmi, S. I., Ertsen, M. W., & Asi, M. R. (2012). The impact of conjunctive use of canal and tube well water in Lagar irrigated area, Pakistan. *Physics and Chemistry of the Earth*, 47–48, 86–98. https://doi.org/10.1016/j.pce.2012.01.001

Kirkham, M. B. (2014). *Principles of soil and plant water relations*. Oxford: Elsevier.

Kottek, M., Grieser, J., Beck, C., Rudolf, B., & Rubel, F. (2006). World map of the Köppen-Geiger climate classification updated. *Meteorologische Zeitschrift*, 15(3), 259–263. https://doi.org/10.1127/0941-2948/2006/0130

Lankford, B. (2006). Localising irrigation efficiency. *Irrigation and Drainage*, 55(4), 345–362. https://doi.org/10.1002/ird.270

Louis, J, Debaecker, V, Pflug, B, Main-Knorn, M, Bieniarz, J, Mueller-Wilm, U, Cadau, E, & Gascon, F. (2016). SENTINEL-2 SEN2COR: L2A processor for users. In *ESA Living Planet Symposium* Prague (pp. 1–8).

McMahon, T. A., Peel, M. C., Lowe, L., Srikanthan, R., & McVicar, T. R. (2013). Estimating actual, potential, reference crop and pan evaporation using standard meteorological data: A pragmatic synthesis. *Hydrology and Earth System Sciences*, 17(4), 1331–1363. https://doi.org/10.5194/hess-17-1331-2013

Mekonnen, M. M., & Hoekstra, A. Y. (2011). The green, blue and grey water footprint of crops and derived crop products. *Hydrology and Earth System Sciences*, 15(5), 1577–1600. https://doi.org/10.5194/hess-15-1577-2011

Muñoz Sabater J. (2019). ERA5-land monthly averaged data from 1981 to present. *Copernicus Climate Change Service (C3S) Climate Data Store (CDS)*.

Narain, V. (2008). Warabandi as a sociotechnical system for canal water allocation: Opportunities and challenges for reform. *Water Policy*, 10(4), 409–422. https://doi.org/10.2166/wp.2008.057

Peters-Lidard, C. D., Mocko, D. M., Garcia, M., Santanello, J. A., Tischler, M. A., Moran, M. S., & Wu, Y. (2008). Role of precipitation uncertainty in the estimation of hydrologic soil properties using remotely sensed soil moisture in a semiarid environment. *Water Resources Research*, 44(5), W05S18. https://doi.org/10.1029/2007WR005884

Priestley, C. H. B., & Taylor, R. J. (1972). On the assessment of surface heat flux and evaporation using large-scale parameters. *Monthly Weather Review*, 100(2), 81–92. https://doi.org/10.1175/1520-0493(1972)100<0081:OTAOSH>2.3.CO;2

Rosenberg, N. J. (1974). *Microclimate: The biological environment*. New York: Wiley.

Schaap, M. G., Leij, F. J., & van Genuchten, M. T. (2001). Rosetta: A computer program for estimating soil hydraulic parameters with hierarchical pedotransfer functions. *Journal of Hydrology*, 251(3–4), 163–176. https://doi.org/10.1016/S0022-1694(01)00466-8

Schulz, S. (2020). Energy balance and soil moisture data of an agricultural test field in Faisalabad, Pakistan. Retrieved from https://doi.pangaea.de/10.1594/PANGAEA.921389

Šimůnek, J., van Genuchten, M. T., & Šejna, M. (2008). Development and applications of the HYDRUS and STANMOD software packages and related codes. *Vadose Zone Journal*, 7(2), 587–600. https://doi.org/10.2136/vzj2007.0077

Šimůnek, J., Šejna, M., Saito, H., Sakai, M., & van Genuchten, M. T. (2013). *The HYDRUS-1D software package for simulating the one-dimensional movement of water, heat, and multiple solutes in variably-saturated media*. Riverside: Department of Environmental Sciences University of California Riverside.

Taylor, S. A., & Ashcroft, G. L. (1972). *Physical Edaphology: The physics of irrigated and nonirrigated soils*. New York: W.H. Freeman.

Troutman, B. M. (1983). Runoff prediction errors and bias in parameter estimation induced by spatial variability of precipitation. *Water Resources Research*, 19(3), 791–810. https://doi.org/10.1029/WR019i003p00791

Wang, K., & Dickinson, R. E. (2012). A review of global terrestrial evapotranspiration: Observation, modeling, climatology, and climatic variability. *Reviews of Geophysics*, 50(2), 2011RG000373. https://doi.org/10.1029/2011RG000373

Wesseling, J. G. (1991). Meerjarige simulatie van grondwaterstroming voor verschillende bodemprofielen, grondwatertrappen en gewassen met het model SWATRE. Wageningen.

Wisser, D., Frolking, S., Douglas, E. M., Fekete, B. M., Vörösmarty, C. J., & Schumann, A. H. (2008). Global irrigation water demand: Variability and uncertainties arising from agricultural and climate data sets. *Geophysical Research Letters*, *35*(24), L24408. https://doi.org/10.1029/2008GL035296

Wongkaew, A., Saito, H., Fujimaki, H., & Šimůnek, J. (2018). Numerical analysis of soil water dynamics in a soil column with an artificial capillary barrier growing leaf vegetables. *Soil Use and Management*, *34*(2), 206–215. https://doi.org/10.1111/sum.12423

Zhang, Y., & Schaap, M. G. (2017). Weighted recalibration of the Rosetta pedotransfer model with improved estimates of hydraulic parameter distributions and summary statistics (Rosetta3). *Journal of Hydrology*, *547*, 39–53. https://doi.org/10.1016/j.jhydrol.2017.01.004

SUPPORTING INFORMATION

Additional supporting information may be found online in the Supporting Information section at the end of this article.